Journal of Membrane Science 453 (2014) 312–319

Contents lists available at ScienceDirect

Journal of Membrane Science

journal homepage: www.elsevier.com/locate/memsci

Enhanced mixing in the diffusive boundary layer for energy generation in reverse electrodialysis

David A. Vermaas [a,b], Michel Saakes [a], Kitty Nijmeijer [b,*]

[a] Wetsus, Centre of Excellence for Sustainable Water Technology, P.O. Box 1113, 8900 CC Leeuwarden, The Netherlands
[b] Membrane Science & Technology, University of Twente, MESA+ Institute for Nanotechnology, P.O. Box 217, 7500 AE Enschede, The Netherlands

ARTICLE INFO

Article history:
Received 23 July 2013
Received in revised form
10 October 2013
Accepted 3 November 2013
Available online 15 November 2013

Keywords:
Reverse electrodialysis
Spacers
Corrugated membranes
Concentration polarization
Particle image velocimetry

ABSTRACT

Renewable energy can be obtained from mixing waters with different salinity using reverse electrodialysis (RED). To obtain a high power per membrane area, combined with a low power consumption for pumping the feed water, RED is preferably operated using small intermembrane distances and low flow rates. However, the diffusive boundary layer near the membranes induces a significant (non-ohmic) resistance at lower flow rates. This is even more pronounced when a spacerless design, with profiled membranes, is used. This research presents how the non-ohmic resistance in RED can be reduced, and consequently the obtained power can be increased, without compromising the power consumed for pumping. Experiments were conducted using several designs, with and without mixing promoters such as twisted spacers and additional sub-corrugations on the membrane, to investigate the effect of additional mixing in the diffusive boundary layer on the obtainable power in RED. The results show that these mixing promoters are not effective at the low Reynolds numbers typically used in RED. The distribution of the feed water inflow, however, has a major impact on the non-ohmic resistance. The design with profiled membranes without sub-corrugations has the best performance, which is almost twice the net power density obtained with a design with normal spacers.

1. Introduction

Reverse electrodialysis (RED) is a technology to capture the available energy when waters with different salinity mix, for example where river water is discharged into the sea. This source for renewable energy is unused at the moment, while the theoretical potential is huge. In theory, the global discharge of river water into the sea can generate sufficient electricity to cover the worldwide electricity consumption [1,2]. The relatively low obtained power per membrane area (i.e. power density) so far inhibited commercial application of this technology, although pilot plants to capture salinity gradient energy have been built or are planned [3,4].

The principle of reverse electrodialysis relies on ion exchange membranes, which are selective for either cations (cation exchange membrane, CEM) or anions (anion exchange membrane, AEM). When waters with different salinity are on either side of such a selective ion exchange membrane, a Donnan potential is created over the membrane. When these membranes are stacked alternately, with compartments for seawater or river water in between, the Donnan potentials over each membrane cumulate to a voltage that can be used for electricity generation. The electrodes at both ends of the stack convert the ionic flux into an electrical current, using a (reversible) redox reaction [5,6] or using ion storage in capacitive electrodes [7].

In traditional designs for RED, the power density is limited mainly by the weakly conductive river water compartments [1,8] and the non-conductive spacers in the compartments [9]. The electrical resistance of the river water compartments can be minimized using very thin feed water compartments, at the cost of higher power consumption for pumping the feed water [1,10]. The pumping power is further increased due to the presence of spacers, which create a tortuous flow [1,11,12]. The spacers (often non-conductive polymeric fabrics) are used between the ion exchange membranes to create a constant intermembrane distance and create extra mixing of the flow within the feed water compartments. However, the non-conductive material of the spacers partly covers the membrane area (and the feed water compartment) and disables that area for ion exchange. This is referred to as the spacer shadow effect [9].

A design without spacers can be created using membranes with a corrugation, i.e. profiled membranes [12,13]. Experiments showed that these profiled membranes have a lower ohmic resistance (i.e. AC resistance) and a four times lower pumping power consumption, compared to a similar design with flat membranes and spacers [12]. However, the non-ohmic resistance,

* Corresponding author. Tel.: +31 53 489 4185; fax: +31 53 489 4611.
E-mail address: d.c.nijmeijer@utwente.nl (K. Nijmeijer).

0376-7388/$ - see front matter © 2013 Elsevier B.V. All rights reserved.
http://dx.doi.org/10.1016/j.memsci.2013.11.005

sometimes referred to as concentration polarization, was higher in the case of profiled membranes. This non-ohmic resistance is due to concentration changes in the feed water compartments, which are most pronounced in the diffusive boundary layer near the membrane surface, when an electrical current is allowed. When the non-ohmic resistance of the design with profiled membranes would decrease to the level as for the design with spacers, the net power density would almost double [12].

The high non-ohmic resistance in the absence of spacers was attributed to reduced mixing near the membrane–water interface [12]. The slow refreshment of the feed waters near the membranes lowers the concentration difference over the membrane and therefore decreases the electromotive force. This results in a non-ohmic resistance. Previous research for other applications showed that additional mixing can be obtained using spacers with a twisted (i.e. helical) structure [14–17] or other static mixing spacers [18]. Also spacerless systems can be equipped with mixing promoters, by adding micro-corrugations such as herringbone structures, on the membrane surface [19,20]. This suggests that with such flow geometry a decrease of the non-ohmic resistance in RED could be obtained.

Alternatively or additionally, a poor water distribution within each feed water compartment causes a higher non-ohmic resistance. In a design with spacers, the feed water is homogeneously distributed in all directions in each feed water compartment, while the profiled membranes guide the water through narrow channels. When a local blockage occurs somewhere in a profiled channel (e.g. due to an air bubble or a locally thicker membrane), the whole channel is unavailable, while using a design with spacers the water can re-distribute in case of a local blockage.

To distinguish the cause of the high non-ohmic resistance of profiled membranes, and to improve the obtained power density in RED, this research investigates two novel designs with mixing promoters. One of the mixing promoters includes spacers while the other type of mixing promoter can be used in a spacerless system. These two novel designs are compared with designs with traditional (straight, non-conductive) spacers and traditional profiled membranes. The performance is evaluated by electrical measurements as well as experimental flow visualization for one of the novel designs with mixing promoters. This research reveals the individual effects of different types of mixing promoters, for designs with spacers as well as for designs with profiled membranes. Consequently, this research shows how the (non-ohmic) resistance can be reduced and a significantly higher (net) power density can be obtained in RED.

2. Experimental setup

2.1. RED designs

Four different RED stacks were built, from which two designs comprised flat membranes with a spacer in between the membranes and two designs comprised profiled membranes. The stacks contained several cells, each composed of a CEM, an AEM, a compartment for river water and a compartment for seawater. All designs used commercial Ralex membranes (MEGA, Czech Republic); type CMH-PES was used as CEM and type AMH-PES was used as AEM. Both stacks with spacers were composed of 5 cells and both stacks with profiled membranes were composed of 6 cells. For a fair (scale independent) comparison, the effect of the electrodes was subtracted using a blank measurement with zero cells (i.e. only electrodes, electrode compartments and one CEM that separates the final cell from the electrodes).

The designs with spacers had either symmetrical spacers composed of filaments of 143 μm in both directions (Fig. 1A) or asymmetrical spacers composed of single wires of 64 μm as a weft and two twisted wires of 64 μm as a warp (Fig. 1B). The twisted structure of this warp creates a helical structure. Each feed water compartment contained two layers of this twisted spacers, to obtain a similar thickness as the normal spacers (Table 1). The spacer type, porosity and open area of both spacers are given in Table 1. Both spacer types were not ion-conductive.

Both designs with profiled membranes included straight ridges in the direction of the feed water flow on one side of the membrane. When the membranes were stacked, these ridges created straight channels of 230 μm high and 1 mm in width. These channels were straight and uniform for one design (Fig. 1C),

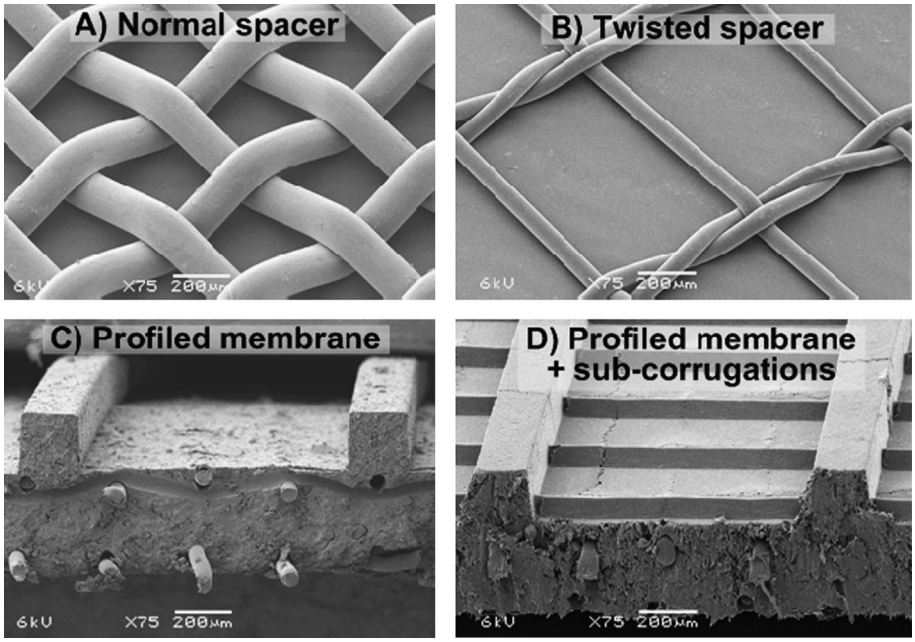

Fig. 1. Images obtained from a scanning electron microscope (SEM, magnification: 75 ×), for normal spacers, twisted spacers and profiled membranes without or with sub-corrugations.

Table 1
Specifications for spacers and membrane profiles.

	Normal spacer	Twisted spacers	Profiled membrane	Profiled membrane + sub-corrugations
Type of spacer	1 layer of Sefar 07-300/46	2 layers of Sefar IEM 07-750/83	No spacer	No spacer
Membrane thickness (wet) (μm)	580 ± 25	580 ± 25	475 ± 15 (excluding profiles)	520 ± 20 (excluding profiles and sub-corrugations)
Compartment thickness (wet) (μm)	245 ± 5	223 ± 7	230 ± 11	230 ± 10
Open area (%)	46	83	83	83
Porosity (%)	72	88	83	81

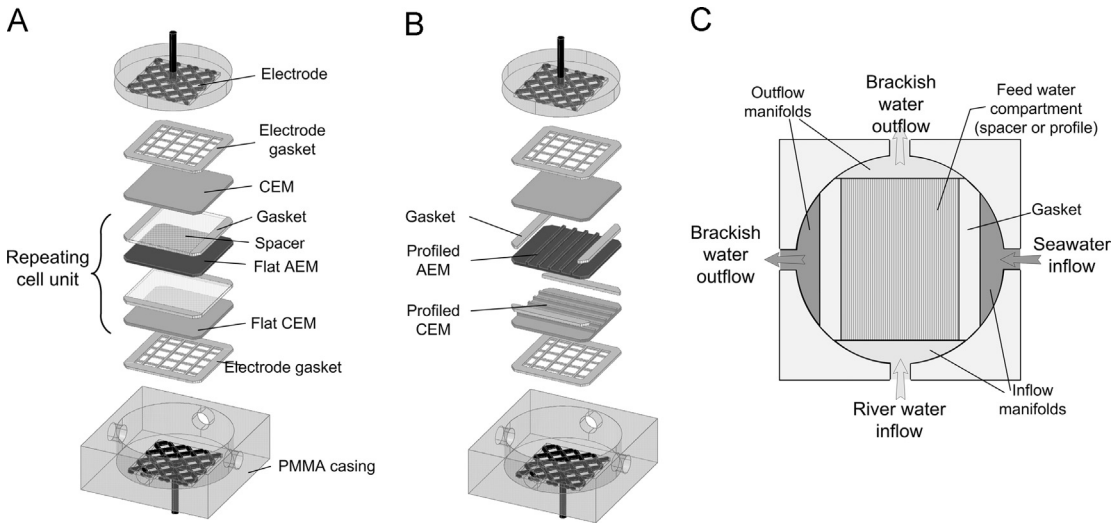

Fig. 2. Composition of RED stacks in case of (A) spacers and (B) profiled membranes (for clarity both stacks are drawn here with only 1 repeating cell unit). (C) represents a cross-sectional top view showing the manifolds and one feed water compartment; in this case a river water compartment. The seawater compartment is oriented perpendicular to the river water compartment.

while the other design had additional, smaller, corrugations in a triangular shape with a height of 50 μm, perpendicular to the flow through the channel (Fig. 1D). These sub-corrugations were added to disturb the uniform flow and create extra mixing in the concentration boundary layer near the membrane surface. To ensure that the sub-corrugations were aligned with the channels created by the larger profiles, the sub-corrugations were only added at one side of the profiled membrane. Both types of profiled membranes (with and without sub-corrugations) were prepared by hot pressing the membranes into a mold, at 140 °C and 200 bar, as explained in more detail in previous research [12]. The membranes were conditioned in 0.5 M NaCl afterwards and the thickness of the membranes and corrugations was measured (Mitutoyo 547-401, Japan); see Table 1.

2.2. Feed water

An artificial solution of 0.508 M NaCl (technical grade, ESCO, The Netherlands) was used as seawater and 0.017 M NaCl was used as river water. These feed waters were supplied through a manifold and such that the flow directions of the feed waters were oriented 90° with respect to each other (i.e. cross-flow), as shown in Fig. 2.

The inflows as depicted in Fig. 2 allowed the feed water to redistribute in the wide manifold and ensured uniform pressure over the full width of the feed water compartments.

The membranes had a dimension of approximately 7 cm by 7 cm. A gasket of 1 cm was used at both sides to prevent river water entering the seawater compartments and vice versa (Fig. 2A and B). Hence, the effective area for ion exchange was 5 cm by 5 cm. All membrane stacks, either with spacers or profiled membranes, were packed between a Ti/Pt mesh electrode of 5 cm by 5 cm (MAGNETO Special Anodes B.V., The Netherlands) and a poly(methyl methacrylate) (PMMA) casing (STT Products, The Netherlands).

The measurements were performed at several flow rates, between 0.5 and 100 ml/min per cell, which are equivalent to Reynolds numbers between 0.5 and 100. The Reynolds number based on half the channel height, Re_h (dimensionless), for a wide channel and corrected for the volume filled by spacer or membrane profile (i.e. including porosity) is defined as

$$Re_h = \frac{\overline{u} D_h \rho}{\mu} \approx \frac{2\Phi\rho}{b\varepsilon\mu} \quad (1)$$

In which $\overline{u}$is the average flow velocity (m/s), D_h is the hydraulic diameter (m), ρ is the density of water (kg/m^3), μ is the (dynamic) viscosity of water (kg/(m•s)), Φ is the flow rate per feed water compartment (m^3/s), b is the width of the feed water compartment (m) and ε is the compartment porosity (dimensionless).

2.3. Electrical measurements

To benchmark the obtained power density obtained in each RED stack, chronopotentiometry was applied. A galvanostat (Ivium Technologies, The Netherlands) was used to measure the voltage at a 0.1 s sample rate for current densities of 4, 8, 12, 16, 20, 24 and 28 A/m^2, each for a duration of at least 4 times the residence time of the feed water, to ensure a stable voltage. Each stage in current density was preceded and followed by a stage with open circuit (open circuit voltage, OCV). The stack resistance (R_{stack}, in Ω cm^2)

is then determined from the difference between the stable voltage at each current density and the OCV. The total electrical resistance of the stack can be divided into an ohmic (R_{ohmic}) and a non-ohmic resistance ($R_{non\text{-}ohmic}$), both in Ω cm^2:

$$R_{stack} = R_{ohmic} + R_{non-ohmic} \quad (2)$$

The ohmic resistance originates from the membrane resistance and the limited conductivity of the feed water. The non-ohmic resistance is due to concentration changes within each compartment, which are oriented perpendicular to the membrane (due to a concentration boundary layer) as well as along the feed water flow (due to a slowly changing bulk concentration). As the ions are transported from the seawater compartment to the river water compartment, the concentration difference over the membranes decreases, which slowly decreases the electromotive force. This decrease in voltage, divided by the current density, determines the non-ohmic resistance.

The ohmic resistance is determined from the sudden jump in voltage when an electrical current is interrupted. The remaining, time-dependent voltage change during the current interrupt is due to the non-ohmic resistance [1].

The obtained gross power density P_{gross} (W/m^2 of membrane area) is calculated from the open circuit voltage (OCV, in V) and the stack resistance:

$$P_{gross} = \frac{OCV^2}{4N_m R_{stack}} \quad (3)$$

in which N_m represents the number of membranes (dimensionless). This paper focuses on the obtained power density rather than the energy efficiency, as the non-ohmic resistance influences the power density unambiguous while the energy efficiency can still be high with significant non-ohmic resistance when using multiple stages [21]. For large scale applications, high energy efficiency can be obtained without compromising the power density when using multiple (small) stages, e.g., using segmented electrodes [22].

All measurements are duplicated, from which the average values and the standard errors are shown.

2.4. Flow visualization

In addition to the electrical measurements in a stack, a cell with a single flow compartment was used to visualize the flow through the channels with sub-corrugations. The flow compartment contained one membrane with sub-corrugations only (approximately 60 μm in height), both at the bottom and top side, glued to a PMMA casing. These membranes only contained the sub-corrugations without the larger corrugations, such that the flow compartment could be visualized from the side (Fig. 3). A glass window was installed at one side of the cell, to ensure a good optical path. The flow compartment was 4 cm in width, 24 cm in length, and approximately 300 μm in height. A solution with 0.25 M NaCl and polystyrene particles with a diameter of 5 μm (Dantec Dynamics, Denmark) was pumped through the flow compartment.

A light source was installed at one side of the flow compartment, while a high-speed camera (Photron Fastcam SA1.1, United States) was installed at the other side. Images were recorded using a resolution of 1024 pixels × 1024 pixels, corresponding to an image size of approximately 1.5 mm. Frame rates of 250 fps ($Re_h = 10$) and 2000 fps ($Re_h = 100$) were used. The movement of the microparticles in two subsequent images was used to calculate the local flow velocity, using a technique known as particle tracking velocimetry (PTV). Approximately 5000 subsequent images were processed to obtain an average flow field. The images were processed in Matlab (Mathworks, v2010b), searching for cross-correlation peaks of tracked particles, with an interrogation window of 64 pixels. A time-average vector field was created by distributing the vectors over a regular grid of 80 × 80, which corresponds to a final resolution of 19 μm.

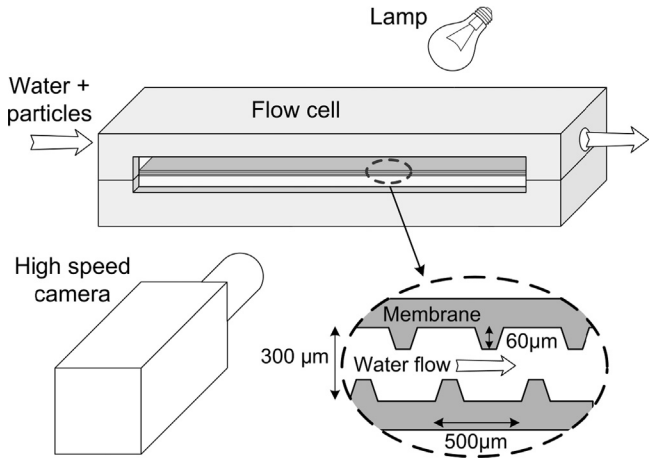

Fig. 3. Experimental setup for flow visualization.

3. Results

3.1. Power density

The experimentally obtained gross power density is shown in Fig. 4 as a function of the Reynolds number for all four designs.

As expected, the gross power density increases with increasing Reynolds number (Fig. 4). The concentration difference over each membrane remains highest when seawater and river water are rapidly refreshed (i.e. high Re_h). For lower Reynolds numbers, thus lower flow rates, the ion transport from seawater compartments to river water compartments lowers the salinity difference over the membrane and therefore lowers the gross power density. In other words, the non-ohmic resistance decreases when the Reynolds number increases, and hence the power density increases.

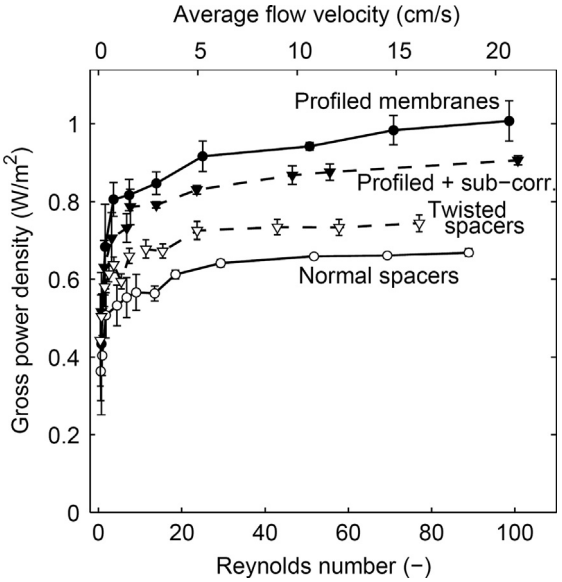

Fig. 4. Gross power density for RED-stacks with normal spacers, twisted spacers, profiled membranes and profiled membranes with additional sub-corrugations as function of the Reynolds number.

The stack with twisted spacers has a significantly higher power density than the stack with normal spacers. However, the stack with profiled membranes with sub-corrugations obtains a slightly lower power density than when profiled membranes without sub-corrugations are used. Although both twisted spacers and sub-corrugations were expected to generate more mixing, i.e. a lower non-ohmic resistance, and thus a higher power density, the effect of these mixing promoters on the power density is contradictive. To investigate this in more detail, the ohmic and non-ohmic resistance are analyzed and discussed in more detail hereafter.

3.2. Ohmic resistance

The total electrical resistance of the stack is decomposed into an ohmic and a non-ohmic resistance, according to Eq. (2). The ohmic resistance, due to the membrane resistance and the ohmic resistance in the feed water compartments, is shown as a function of Re_h for all designs in Fig. 5.

Fig. 5 shows that the ohmic resistance is rather independent of the Reynolds number, as was demonstrated also in previous research [9,12]. The ohmic resistance is only slightly lower for very low Reynolds numbers, which is caused by the higher conductivity of the river water compartments. This effect is strongest for low Reynolds numbers, because lower flow rates imply larger residence times, which result in accumulated transport of ions from the seawater into the river water compartments. Since the low conductive river water compartment contributes more to the ohmic resistance than the seawater compartment, the ohmic resistance slightly decreases at low Reynolds numbers.

The stack with twisted spacers shows a significantly lower ohmic resistance than the stack with normal spacers. This is due to the more open structure of the twisted spacer, which can be quantified by the higher open area and porosity, compared to the normal spacers (Table 1). The more open structure of the twisted spacers reduces the spacer shadow effect. Therefore, the ohmic resistance is lower for the stack with twisted spacers in comparison to that with normal spacers. In addition, the twisted spacers are slightly thinner than the normal spacers, which would give a little lower resistance for the compartments filled with twisted spacers than those with normal spacers [1]. Based on previous research [10], the difference in spacer thickness decreases R_{ohmic} by approximately 5%, and consequently the difference in open area and porosity are responsible for the latter 15% decrease in R_{ohmic} for the stack with twisted spacers, relative to stack with normal spacers.

Both designs with profiled membranes have a lower ohmic resistance than both designs with spacers (Fig. 5). This is due to the absence of the spacer shadow effect in stacks with profiled membranes, as the use of (non-conductive) spacers is obsolete in the designs with profiled membranes. The difference in ohmic resistance between the stacks with profiled membranes and the stack with normal spacers is even more pronounced than demonstrated in previous research [12], which is caused by the slightly thicker membranes (i.e. higher resistance) for the stack with spacers compared to the thinner profiled membranes (Table 1). Considering the actual differences in membrane resistance (approximately 5 $\Omega\,cm^2$ higher for the cells with normal spacers compared to previous research), these results are in fair agreement with previous research [12]. In all cases, the stacks with spacers have a significant higher ohmic resistance than the stack with profiled membranes.

The stack with additional sub-corrugations has a slightly higher ohmic resistance than the stack with profiled membranes without sub-corrugations, although this difference is only significant for a few data points (Fig. 5). The small differences in ohmic resistance of this stack with sub-corrugations re attributed to the slightly thicker profiled membranes with sub-corrugations, compared to the profiled membranes without sub-corrugations (Table 1).

3.3. Non-ohmic resistance

The non-ohmic resistance ($R_{non\text{-}ohmic}$) as a function of Re_h is shown for all designs in Fig. 6.

The ohmic resistance (Fig. 5) dominates the non-ohmic resistance (Fig. 6) for all Reynolds numbers and all cases. At a moderate flow rate corresponding to $Re_h = 10$, R_{ohmic} is approximately 3.5 times higher than $R_{non\text{-}ohmic}$ for designs with profiled membranes, and even 10 times higher for designs with spacers.

Furthermore, the non-ohmic resistance (Fig. 6) decreases strongly with increasing Reynolds number. Since the non-ohmic resistance is due to concentration changes within the feed water compartments, the non-ohmic resistance decreases when the

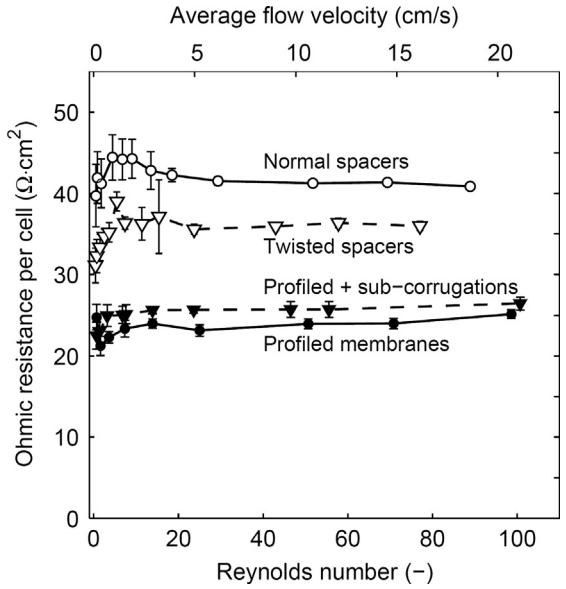

Fig. 5. Ohmic resistance per cell for RED-stacks with normal spacers, twisted spacers, profiled membranes and profiled membranes with additional sub-corrugations as function of the Reynolds number.

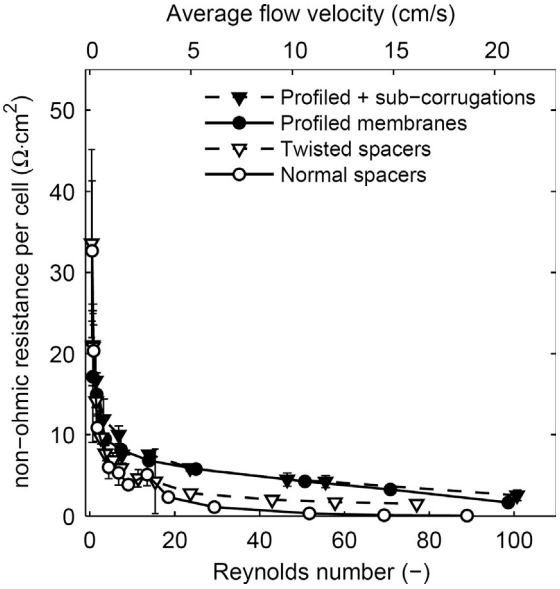

Fig. 6. Non-ohmic resistance per cell for RED-stacks with normal spacers, twisted spacers, profiled membranes and profiled membranes with additional sub-corrugations as function of the Reynolds number.

residence time is lower, i.e. when the feed water flow is higher. Moreover, higher Reynolds numbers imply higher velocity shears near the membrane–water interface, which decrease the concentration boundary layer (i.e. diffusive boundary layer) [23]. In other words, the concentration near the membrane–water interface is more similar to the inflow concentrations for higher flow rates, and consequently the non-ohmic resistance decreases for higher Reynolds numbers.

The non-ohmic resistances of the stacks with twisted spacers and sub-corrugations are similar or even higher than those for the comparable designs with normal spacers and profiled membranes without sub-corrugations. This result shows that the obtained power cannot be improved by adding these types of mixing promoters (twisted spacers and sub-corrugation) to reduce the non-ohmic resistance.

Previous research on (multilayer) spacers did show significant improvement in mass transfer using helical spacer structures [14,15]. The absence of a decrease in $R_{\text{non-ohmic}}$ for the designs with twisted spacers and sub-corrugations in the present research can be explained by two factors. First of all, the distribution of the feed water inflow dominates $R_{\text{non-ohmic}}$. The non-ohmic resistances for the stacks with normal spacers and profiled membranes (without sub-corrugations) are much lower in this research than in previous research with such stacks at similar residence time [12]; 27% lower for normal spacers and 44% lower for profiled membranes. This decrease is due to an improved flow design with a wide inflow and outflow manifold for the feed water, whereas previous research used a single hole for the inflow of each feed water type [12]. Wide manifolds ensure a more uniform feed water distribution over the membrane area, while inflow and outflow from a single point as in previous research can create more preferential channeling and dead zones [24]. This effect is major, as demonstrated by the significant decrease in $R_{\text{non-ohmic}}$ in this research compared to previous research. In other words, the additional mixing that is generated due to the twisted spacers, for example, is insignificant compared to the effect of the feed water distribution over the membrane.

A second reason why the twisted spacers and sub-corrugations do not reduce $R_{\text{non-ohmic}}$ is the low Reynolds numbers that are typically used in RED. Previous research on helical spacer structures [14,15] was performed at $Re_h > 100$, while RED is typically operated at $Re_h < 100$ and preferably even $Re_h < 10$ [1,10,12]. At higher Reynolds numbers, unsteady vortices could be generated from disturbances such as spacer filaments or sub-corrugations [14,25,26]. Vortices at $Re_h < 100$ are reported in spacer-filled channels [14,26], but are steady and limited to a small region near the spacer yarn only. Consequently, the effect is minor.

3.4. Flow visualization

To visualize the feed water flow at the relatively low Reynolds numbers that are typical for RED, particle tracking velocimetry (PTV) was applied for the case with sub-corrugations. The experimentally obtained, time averaged, flow field of the design with sub-corrugations is shown in Fig. 7 for the case with $Re_h = 10$ and $Re_h = 100$.

Fig. 7 shows that the flow bends around the sub-corrugations at both Reynolds numbers. The flow velocity at the tips of the sub-corrugations is lower compared to that at positions in between two sub-corrugations at the same height for $Re_h = 10$, whereas at $Re_h = 100$ the velocity magnitude is even highest near the top of the sub-corrugations (indicated by the yellow or darker gray color near the sub-corrugations at the top). At low flow rate ($Re_h = 10$), the water can follow the geometry of the sub-corrugated membranes, while at high flow rates the inertia of the water is larger and the flow is funnelled near the sub-corrugations, which produces a locally intensified flow velocity near the membrane surface. However, the flow is still fully laminar in both cases. The local minima and maxima in velocity magnitude near the centerline of the compartment are insignificant (due to particles out of focus). No vortices are observed behind the sub-corrugations, as shown in Fig. 7, not for $Re_h = 10$ and neither for $Re_h = 100$. The sub-corrugations create a dead zone in front and behind the

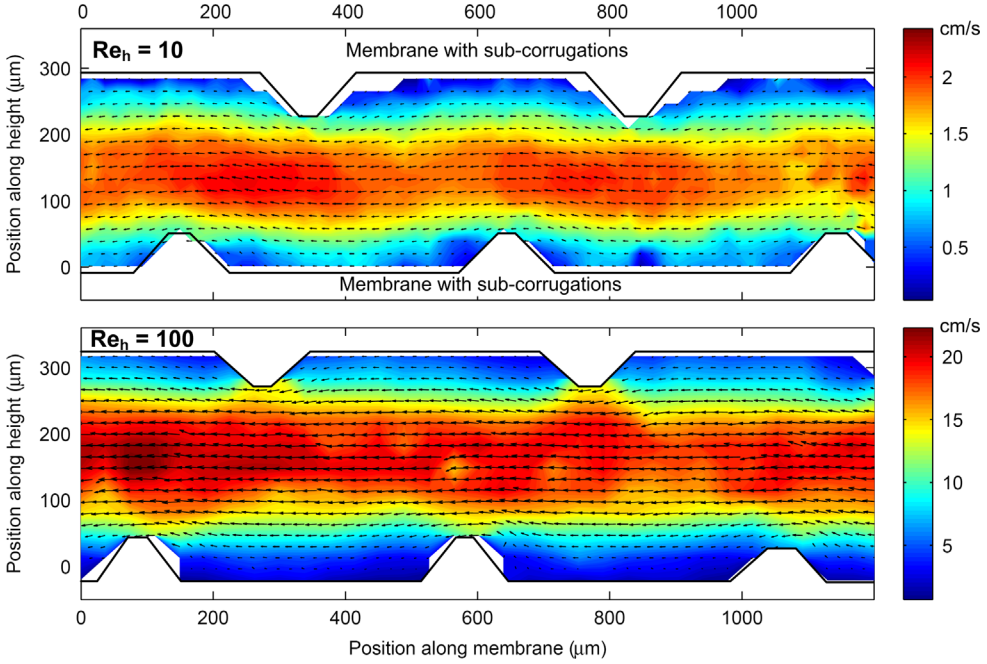

Fig. 7. Experimentally obtained velocity field of flow between sub-corrugated membranes for $Re_h = 10$ and $Re_h = 100$. The colors indicate the velocity magnitude in cm/s, while the vectors indicate the flow direction and magnitude. The shading indicates the velocity magnitude in cm/s, while the vectors indicate the flow direction and magnitude. (For interpretation of the references to color in this figure legend, the reader is referred to the web version of this article.)

sub-corrugations, rather than introducing additional mixing due to vortices. Therefore, sub-corrugations are not suitable to promote mixing in the diffusive boundary layer in RED.

Higher Reynolds numbers could generate vortices in the diffusive boundary layer, but higher flow rates are unfavorable for application in RED due to the corresponding increase in power consumed for pumping [1]. Higher Reynolds numbers can be applied in electrodialysis (ED) applications, which is in general associated with larger intermembrane distances. As a consequence, these sub-corrugations may be useful to generate extra mixing for ED. Moreover, corrugated surfaces are known to enhance the onset for the overlimiting current (i.e. a lower voltage is required to start an overlimiting current) in cases of ED [27]. As RED always operates at underlimiting current, in absence of phenomena such as electroconvection [28], this effect does not benefit the obtained power in RED.

3.5. Net power density

The previous results showed that the feed water distribution throughout each compartment, regulated by the inflow and outflow, mainly determines the non-ohmic resistance. The system for inflow and outflow also influences the pressure drop over the feed water compartments, and thus the net power density (i.e. the obtained gross power density minus the power density consumed for pumping the feed waters). The pressure drop and the net power density for the four stacks investigated are shown in Fig. 8 as a function of the Reynolds number.

Both designs with profiled membranes have a pressure drop which is close to the theoretical pressure drop for laminar flow in a (finite) rectangular channel, considering the porosity (ε) and the finite width [10,29]. The small difference between the theoretical pressure drop and the experimentally obtained pressure drop can be due to slight pressure losses in the manifolds distributing the water [30], although this effect is much smaller in the wide manifolds used in this research compared to previous research [12].

The pressure drop, and thus the power consumed for pumping, is nearly an order of magnitude higher for both designs with spacers compared to both designs with profiled membranes (Fig. 8A). The spacer yarns give substantial extra friction to the feed water flow through the compartments, as was observed before [12,31]. The large standard errors of the stacks with spacers, caused by the local (and unpredictable) imprint of the spacers in the membranes, do not allow to conclude which spacer corresponds to the lowest pressure drop. However, despite the slightly thinner spacers, the pressure drop for the twisted spacers can be considered rather lower than higher compared to the normal spacers. The high porosity and the corresponding large warp size seem to compensate for the slightly smaller thickness of the twisted spacers (Table 1).

The high pressure drops for the stacks with spacers (Fig. 8A) are indirectly related to the low non-ohmic resistances for those stacks (Fig. 6). The high pressure drop in the spacer filled compartment ensures a more uniform flow distribution, as the pressure drop in the manifolds becomes insignificant [30]. Therefore, the feed water distributes more evenly over the full width of the feed water compartments, which reduces the non-ohmic resistance. As a consequence, the stacks with the lowest pressure drops rank opposite for the non-ohmic resistance.

Due to the higher gross power and the relatively low pumping power consumption for stacks with profiled membranes, the net power density is significantly higher for stacks with profiled membranes than for stacks with spacers, as shown in Fig. 8B. The net power densities for the stacks with profiled membranes are higher compared to previous research, due to the improved feed water design in the present research. The net power density is maximum 0.8 W/m^2, which is almost twice the maximum net power density for the stack with normal spacers, and approximately 40% higher compared to the stack with (highly porous) twisted spacers. The addition of sub-corrugations results in general in a slightly lower net power density. Therefore, the use of sub-corrugations is considered not beneficial for RED.

4. Conclusions

This research investigates the power density obtained from mixing seawater and river water solutions in reverse electrodialysis (RED) using designs with and without mixing promoters in the feed water to reduce the diffusive boundary layer. RED stacks with spacer yarns in a twisted structure outperform stacks with normal spacers, due to a higher open area and porosity of the twisted spacers. However, the non-ohmic resistance, which was expected to reduce due to additional mixing in the case of the twisted spacers, was similar to or even higher than that for stacks with normal spacers. For a spacerless design with profiled membranes, the addition of 50 μm sub-corrugations on the membrane

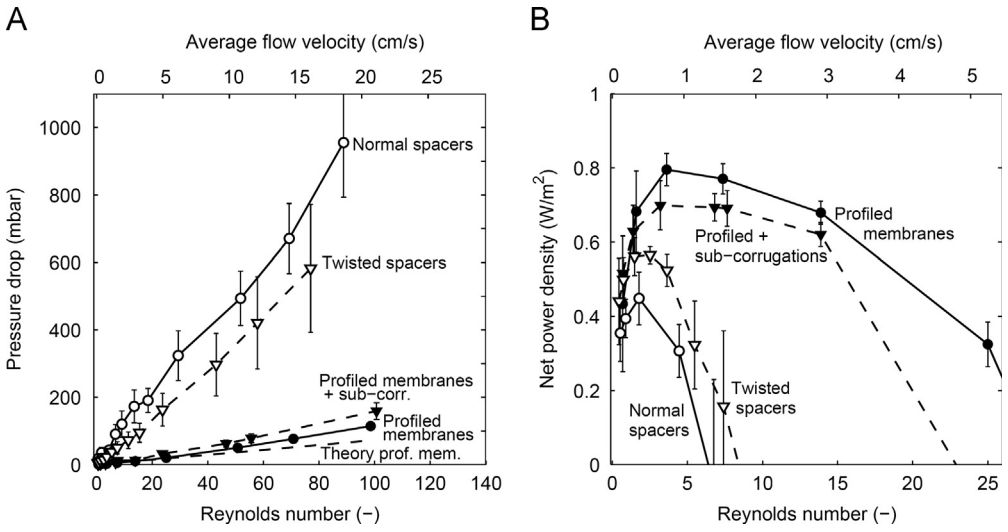

Fig. 8. (A) Pressure drop over feed water compartment and (B) net power density for all designs of this research as a function of the Reynolds number. The shown theoretical pressure drop in panel A corresponds to the case of profiled membranes.

surface as mixing promoters also did not show a decrease in non-ohmic resistance. Flow visualization of the profiled membrane with additional sub-corrugations showed that the corrugated surface does not create vortices at typical Reynolds numbers for RED applications ($Re_h \leq 100$). Moreover, the non-ohmic resistance is sensitive for the flow distribution of the feed water. Ensuring a uniform feed water flow by providing wide manifolds for the distribution of the feed water makes the non-ohmic resistance inferior to the ohmic resistance in all cases. Therefore, mixing promoters such as twisted spacers or sub-corrugations do not yield additional mixing that results in a significantly higher power density for RED. Overall, considering the net power density, stacks with profiled membranes without sub-corrugations perform slightly better than the design with additional sub-corrugations and outperform stacks with spacers with 40% or even more.

Acknowledgments

This research is performed at Wetsus, Technological Top Institute for Water technology (www.wetsus.nl). Wetsus is funded by the Dutch Ministry of Economic Affairs, the European Union Regional Development Fund, the Province of Fryslân, the City of Leeuwarden and the EZ/Kompas program of the 'Samenwerkingsverband Noord-Nederland'. The authors are thankful for the support of the participants of the research theme 'Blue Energy'. The authors also thank Arie Zwijnenburg for creating SEM-images (Fig. 1), Damnearn (Don) Kunteng for his assistance in performing the experiments and Odne Burheim for fruitful discussions.

References

[1] D.A. Vermaas, M. Saakes, K. Nijmeijer, Double power densities from salinity gradients at reduced intermembrane distance, Environ. Sci. Technol. 45 (2011) 7089–7095.
[2] P.E. Długołęcki, A. Gambier, K. Nijmeijer, M. Wessling, Practical potential of reverse electrodialysis as process for sustainable energy generation, Environ. Sci. Technol. 43 (2009) 6888–6894.
[3] J.W. Post, C.H. Goeting, J. Valk, S. Goinga, J. Veerman, P.J.F.M. Hack, Towards implementation of reverse electrodialysis for power generation from salinity gradients, Desalin. Water Treat. 16 (2010) 182–193.
[4] A. Achilli, A.E. Childress, Pressure retarded osmosis: from the vision of Sidney Loeb to the first prototype installation – review, Desalination 261 (2010) 205–211.
[5] J. Veerman, M. Saakes, S. Metz, G. Harmsen, Reverse electrodialysis: evaluation of suitable electrode systems, J. Appl. Electrochem. 40 (2010) 1461–1474.
[6] O.S. Burheim, F. Seland, J.G. Pharoah, S. Kjelstrup, Improved electrode systems for reverse electro-dialysis and electro-dialysis, Desalination 285 (2012) 147–152.
[7] D.A. Vermaas, S. Bajracharya, B.B. Sales, M. Saakes, B. Hamelers, K. Nijmeijer, Clean energy generation using capacitive electrodes in reverse electrodialysis, Energy Environ. Sci. 6 (2013) 643–651.
[8] R.E. Lacey, Energy by reverse electrodialysis, Ocean Eng. 7 (1980) 1–47.
[9] P.E. Długołęcki, J. Dąbrowska, K. Nijmeijer, M. Wessling, Ion conductive spacers for increased power generation in reverse electrodialysis, J. Membr. Sci. 347 (2010) 101–107.
[10] D.A. Vermaas, E. Guler, M. Saakes, K. Nijmeijer, Theoretical power density from salinity gradients using reverse electrodialysis, Energy Proc. 20 (2012) 170–184.
[11] J. Veerman, M. Saakes, S.J. Metz, G.J. Harmsen, Reverse electrodialysis: a validated process model for design and optimization, Chem. Eng. J. 166 (2011) 256–268.
[12] D.A. Vermaas, M. Saakes, K. Nijmeijer, Power generation using profiled membranes in reverse electrodialysis, J. Membr. Sci. 385–386 (2011) 234–242.
[13] J. Balster, D.F. Stamatialis, M. Wessling, Membrane with integrated spacer, J. Membr. Sci. 360 (2010) 185–189.
[14] F. Li, G.W. Meindersma, A.B.D. Haan, T. Reith, Novel spacers for mass transfer enhancement in membrane separations, J. Membr. Sci. 253 (2005) 1–12.
[15] J. Balster, I. Pünt, D.F. Stamatialis, M. Wessling, Multi-layer spacer geometries with improved mass transport, J. Membr. Sci. 282 (2006) 351–361.
[16] A. Shrivastava, S. Kumar, E.L. Cussler, Predicting the effect of membrane spacers on mass transfer, J. Membr. Sci. 323 (2008) 247–256.
[17] C. Fritzmann, M. Hausmann, M. Wiese, M. Wessling, T. Melin, Microstructured spacers for submerged membrane filtration systems, J. Membr. Sci. 446 (2013) 189–200.
[18] J. Liu, A. Iranshahi, Y. Lou, G. Lipscomb, Static mixing spacers for spiral wound modules, J. Membr. Sci. 442 (2013) 140–148.
[19] A.D. Stroock, S.K.W. Dertinger, A. Ajdari, I. Mezic, H.A. Stone, G.M. Whitesides, Chaotic mixer for microchannels, Science 295 (2002) 647–651.
[20] J.D. Kirtland, G.J. McGraw, A.D. Stroock, Mass transfer to reactive boundaries from steady three-dimensional flows in microchannels, Phys. Fluids 18 (2006) 1–13.
[21] J.W. Post, H.V.M. Hamelers, C.J.N. Buisman, Energy recovery from controlled mixing salt and fresh water with a reverse electrodialysis system, Environ. Sci. Technol. 42 (2008) 5785–5790.
[22] D.A. Vermaas, J. Veerman, N.Y. Yip, M. Elimelech, M. Saakes, K. Nijmeijer, High efficiency in energy generation from salinity gradients with reverse electrodialysis, Sustain. Chem. Eng. 1 (2013) 1295–1302.
[23] P.E. Długołęcki, P. Ogonowski, S.J. Metz, M. Saakes, K. Nijmeijer, M. Wessling, On the resistances of membrane, diffusion boundary layer and double layer in ion exchange membrane transport, J. Membr. Sci. 349 (2010) 369–379.
[24] M.C. Hatzell, B.E. Logan, Evaluation of flow fields on bubble removal and system performance in an ammonium bicarbonate reverse electrodialysis stack, J. Membr. Sci. 446 (2013) 449–455.
[25] A.L. Ahmad, K.K. Lau, M.Z.A. Bakar, Impact of different spacer filament geometries on concentration polarization control in narrow membrane channel, J. Membr. Sci. 262 (2005) 138–152.
[26] C.P. Koutsou, S.G. Yiantsios, A.J. Karabelas, Numerical simulation of the flow in a plane-channel containing a periodic array of cylindrical turbulence promoters, J. Membr. Sci. 231 (2004) 81–90.
[27] J. Balster, M.H. Yildirim, D.F. Stamatialis, R. Ibanez, R.G.H. Lammertink, V. Jordan, M. Wessling, Morphology and microtopology of cation-exchange polymers and the origin of the overlimiting current, J. Phys. Chem. B 111 (2007) 2152–2165.
[28] C.L. Druzgalski, M.B. Andersen, A. Mani, Direct numerical simulation of electroconvective instability and hydrodynamic chaos near an ion-selective surface, Phys. Fluids 25 (2013) 110804.
[29] M. Bahrami, M.M. Yovanovich, J.R. Culham, Pressure drop of fully-developed, laminar flow in microchannels of arbitrary cross-section, J. Fluids Eng. 128 (2006) 1036–1044.
[30] L. Gurreri, A. Tamburini, A. Cipollina, G. Micale, CFD analysis of the fluid flow behavior in a reverse electrodialysis stack, Desalin. Water Treat. 48 (2012) 390–403.
[31] A.R. Da Costa, A.G. Fane, D.E. Wiley, Spacer characterization and pressure drop modelling in spacer-filled channels for ultrafiltration, J. Membr. Sci. 87 (1994) 79–98.